ELSEVIER

Surface Science 418 (1998) 32–45

surface science

Direct methods determination of the Si(111)-(6 × 6)Au surface structure

D. Grozea [a,*], E. Landree [a], L.D. Marks [a], R. Feidenhans'l [b], M. Nielsen [b], R.L. Johnson [c]

[a] *Department of Materials Science and Engineering, Northwestern University, Evanston, IL 60208, USA*
[b] *Department of Solid State Physics and Chemistry, Risø National Laboratory, DK-4000 Roskilde, Denmark*
[c] *II. Institute for Experimental Physics, University of Hamburg, 22761 Hamburg, Germany*

Received 2 April 1998; accepted for publication 31 July 1998

Abstract

The atomic structure of the Au 6 × 6 on Si(111) phase has been determined using direct methods and surface X-ray diffraction data. This surface structure is very complicated, with 14 independent gold atoms, relaxations in 24 independent silicon sites and three partially occupied gold sites. In one sense the structure can be described as microdomains of the parent $\sqrt{3} \times \sqrt{3}$ Au on Si(111) structure. A better description is in terms of a tiling of incomplete pentagonal and trimer units, essentially a pseudo-pentagonal glass. In terms of these structural units it is possible to explain all the gold structures in the coverage range 0.8–1.5 monolayers as pseudo-glasses with strong short-range order but varying degrees of long-range order.

Keywords: Computer simulations; Direct methods; Gold; Low index single crystal surfaces; Si(111)-(6 × 6)Au; Silicon; Surface relaxation and reconstruction; X-ray diffraction

1. Introduction

The gold on Si(111) surface in the coverage range 0–2 monolayers (ML) has been extensively studied, but many of the details are still unclear and the underlying physics uncertain. Below one monolayer two distinct phases, the 5 × 2 [1] and $\sqrt{3} \times \sqrt{3}$ [2] structures, are known to exist. Both of these are stable to temperatures far in excess of the unusually low bulk eutectic melting point of 363°C. In this coverage regime, a new approach has provided a better understanding of surface structures. Plass and Marks [3] proposed a phase diagram for submonolayer Au on Si(111) system, obeying Gibbs phase rules and with phase boundaries based on thermodynamics principles. This approach for surfaces is replacing the more familiar phase maps, which show the temperature versus coverage regime for surface phases. Extending the surface phase diagram to higher Au coverages requires knowledge of the atomic structure of the surface phases present above 1 ML of Au.

In the range 1.0–1.5 ML (and perhaps with slightly lower coverages) diffraction experiments show strong $\sqrt{3} \times \sqrt{3}$ intensities and additional diffuse or ordered structures [4–10]. Star-like spots and sharp spots surrounded by ring-like structures

* Corresponding author. Fax: +1 847 4917820; e-mail: dgrozea@merle.acns.nwu.edu

0039-6028/98/$ – see front matter
PII: S0039-6028(98)00660-8

(simple diffuse rings, rings with a double-spot hexagon pattern, or incomplete rings) have been observed. The best defined of these structures is the Au 6×6 surface phase occurring around 1.4 ML coverage, which forms very close to the bulk eutectic temperature. However, other studies [11,12] have reported the formation of the 6×6 structure at 1.0 ML, thus the exact Au coverage is still controversial. At higher coverages gold particles form, suggesting a Stranski–Krastanov growth mode [4,13], although Święch et al. [14] reported the formation of 3D Au particles as preceding and continuing in parallel with the 6×6 structure formation and growth.

It should be noted that quenching the bulk eutectic is known to produce a glass [15] which appears to crystallize at similar temperatures into a number of poorly determined phases [16–18]. In addition, there is some evidence from X-ray photoelectron spectroscopy [19], low-energy electron diffraction (LEED) [20], and reflection high-energy electron diffraction (RHEED) [21] data for a gold-silicide. Understanding the Au 6×6 structure can shed light on the transition from a 2D surface to a more bulk behavior. Furthermore, because the temperatures are very close to the bulk eutectic and glass formation/crystallization temperatures, unusual phenomena may be present. For instance, in this temperature and coverage range strong homoepitaxial growth of silicon has been observed [22].

The Au 6×6 phase was first reported by Lander [23] and subsequently studied by almost all surface-sensitive methods: LEED [4,8,11,23], transmission electron diffraction (TED) [6], Auger electron spectroscopy [8,24], Rutherford backscattering spectroscopy [8], X-ray diffraction (XRD) [5], impact-collision ion-scattering spectroscopy (ICISS) [11], and scanning tunneling microscopy (STM) [9,12,24]. Several results indicated that the 6×6 structure is closely connected to the Au $\sqrt{3}\times\sqrt{3}$ structure, and can be considered as a low temperature precursor phase for the unknown surface which displays a $\sqrt{3}\times\sqrt{3}+$ring-like diffraction pattern. Higashiyama et al. [4] found the phase transition between these two structures to be reversible. The Au 6×6 diffraction pattern transformed into the $\sqrt{3}\times\sqrt{3}+$ring-like structure by annealing at high temperature, which again transformed back into the 6×6 structure by annealing at low temperature. Based on a kinematical analysis of LEED spot profiles, the same study suggested that the unusual $\sqrt{3}\times\sqrt{3}$ patterns are due to early stages of the 6×6 phase formation. Using also the STM observations by Salvan et al. [24], which showed the 6×6 surface displaying structural units in which four maxima are arranged with $\sqrt{3}\times\sqrt{3}$ periodicity, Higashiyama et al. [4] explained the reversible transition between the two phases as a gradual ordering/disordering of the structural units. On the other hand, other studies [6,12] found an irreversible transition, with the 6×6 diffraction pattern forming only by additional gold deposition onto the $\sqrt{3}\times\sqrt{3}+$ring-like structure during heating in the low temperature regime.

From ICISS experimental data, Huang and Williams [11] proposed a 6×6 honeycomb structure composed of a centered hexagonal array with 25% empty hexagons. Thus, the structure is consistent with the honeycomb model for $\sqrt{3}\times\sqrt{3}$, which they considered to be a precursor and an incomplete 6×6 phase with centered and empty hexagons lacking long-range order. An STM study [12] of the 6×6 structure, formed at a gold coverage slightly above 1 ML, shows sets of three maxima surrounded by triangular domain walls and a number of bright "protrusions". In this model the 6×6 structure is described as a periodic arrangement of small $\sqrt{3}\times\sqrt{3}$ domains. At a higher coverage (1.4 ML), another STM paper [9] suggested a slightly different structure, a rectangular array of protrusions with a smaller periodicity than the 6×6 unit cell.

A previous attempt to look at this surface using X-ray diffraction data and a Patterson approach was at best only partially successful [5]. The Patterson method generates maps which show positive peaks corresponding to interatomic vectors. The map analysis may provide information on only part of the structure due to the difficulty of picking out individual interatomic vectors and the presence of artifacts. In addition, false peaks may arise by special relationships between interatomic vectors. However, the Patterson map clearly showed that Au trimers are an essential part of the structure. This X-ray study concluded that the

6×6 phase is not an ordered superstructure of the $\sqrt{3} \times \sqrt{3}$, and the main feature of their model was Au trimer triplets.

Despite extensive study, the Au $6 \times 6'$ atomic structure remains unclear. We report here the use of direct methods to determine the atomic structure of the Au 6×6 surface. Key points of the structure and preliminary results have been published in ref. [25].

2. Direct methods

At the moment there are no techniques which can image the atomic structure of a surface in a straightforward manner. While STM does offer some information regarding the outmost layer of atoms, it shows only the density of surface states, and does not provide actual atom positions. Another surface technique, high resolution transmission electron microscopy (HREM), can provide detailed atomic scale imaging. However, HREM information is tedious to acquire, and the signal to noise ratio is often extremely low.

Diffraction techniques, while being very powerful for accurate refinement of the atomic positions, necessitate a starting model that is close to the "correct" structure since they only determine the structure factor amplitudes. In order to restore the charge density or scattering potential (X-ray or electron diffraction respectively), it is necessary to recover the phase of the structure factors. The standard method for doing this with bulk crystals is to use what are called direct methods [26], a technique which has recently also been applied to electron diffraction data [27]. This approach is now being applied with success to provide an initial guess for the solution of surface structures using both electron and X-ray surface diffraction data [28–34]. In effect, direct methods solve the phase problem by exploiting probability relationships which exist between the amplitudes and phases of the diffracted beams.

The direct methods approach we used for solving the Au 6×6 structure involved a minimum relative entropy method with windowed unitary structure factors and a normalized robust figure of merit, coupled with a genetic algorithm for global optimization (for more details see refs. [32–35]). A search is performed to find phase estimates for the measured intensities which satisfy self-consistent conditions, defined by the figure of merit (FOM). Output is a list of plausible solutions, phasing maps obeying the imposed symmetry, ranked in order of the FOM. These are then used as starting points for constructing possible atomic models of the surface structure. In effect, the method generates a set of plausible atomic solutions for the structure, avoiding the need to guess, starting just from the intensity data. Ideally, with small or no experimental measurement errors, and a complete set of intensities, these phasing maps will be accurate restorations of the charge density. In practice, sometimes only part of the structure is identifiable in the initial analysis, the case herein since the true structure is $p3$ with twinning. However, even with a relatively small fragment of the structure known, the remainder can be uniquely determined by one of many different methods; more details of the particular approach we used are given below.

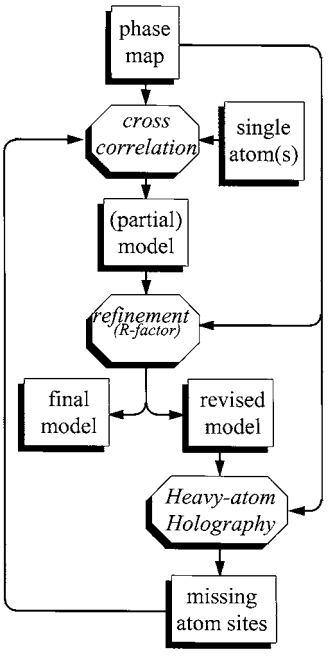

Fig. 1. Flow chart of the iteration process of atomic position refinement/heavy-atom holography.

3. Results

Details of the collection of the X-ray intensity data have been previously reported [5] and will not be described herein. A total of 139 independent intensities in the *p6mm* plane group and 248 in the *p3* plane group were used.

Working from an initial fragment identifiable in the phasing maps, the full structure was determined by combining iterative steps of refinement of the atomic positions and heavy-atom holography [1] to determine new sites, Fig. 1. Cross-correlation of a charge density map for a single atom (Au in this case) with the phasing map generated by the direct methods produces a new map, highlighting the most likely atom positions within the unit cell. The program lists all the possible sites in decreasing order of intensity. The initial fragment of the structure is built by placing atoms at the most intense peaks in the cross-correlation map. The effect of adding each new atom to the structure is monitored by calculating diffraction intensities for the new fragment thus created and comparing these to the measured intensities. After a refinement (*R*-factor type) of the atomic positions, new possible atomic sites are generated using the heavy-atom holography algorithm. These sites are also listed in decreasing order of intensity and only the most intense possible positions are selected during each iteration. Again, diffraction intensities are

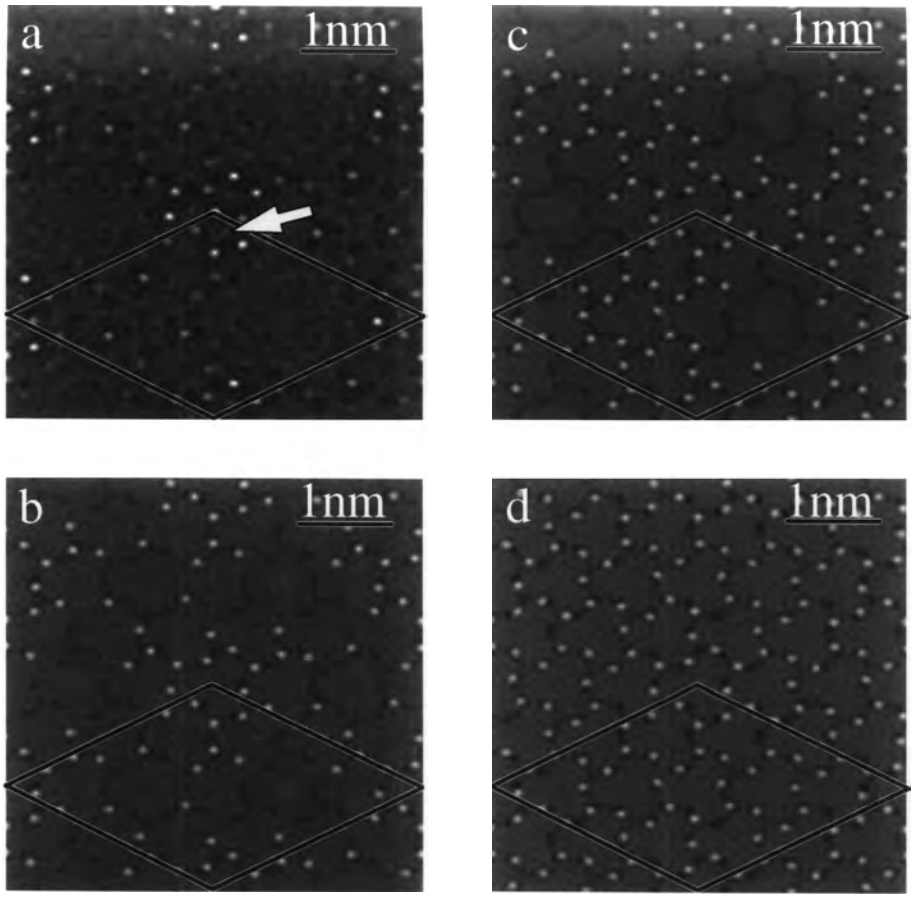

Fig. 2. (a) Phase map of the initial fragment first used with the primitive unit cell indicated by solid lines (unit cell length 6*a*, $a=$ 3.83 Å). A weaker Si site (one of the three symmetry equivalent) is arrowed, all other peaks correspond to Au sites; (b, c) intermediate steps in constructing the model; (d) final model with 42 gold atoms.

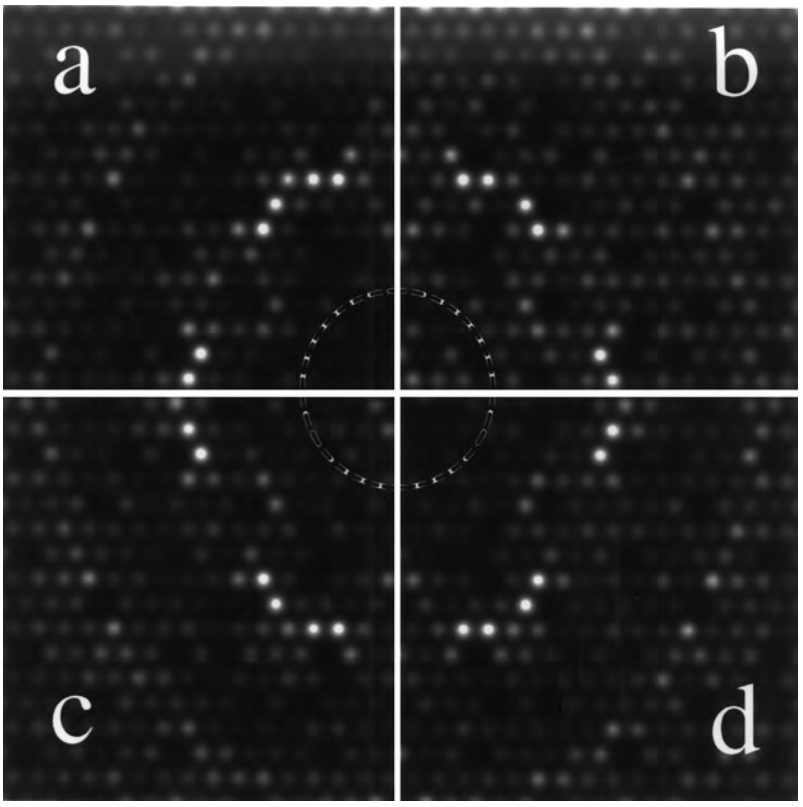

Fig. 3. (a–d) Corresponding diffraction patterns for Fig. 2a–d. The dashed circle is added to highlight a region where some beam intensities vary at different stages of model completion.

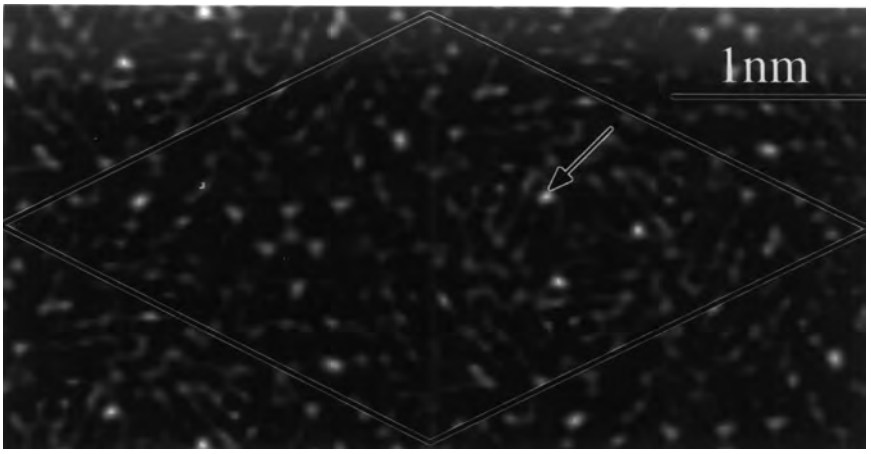

Fig. 4. New possible atom sites generated by heavy-atom holography after processing the partial model from Fig. 2c. The most intense sites were chosen as the next step (one of the three symmetry equivalents is arrowed).

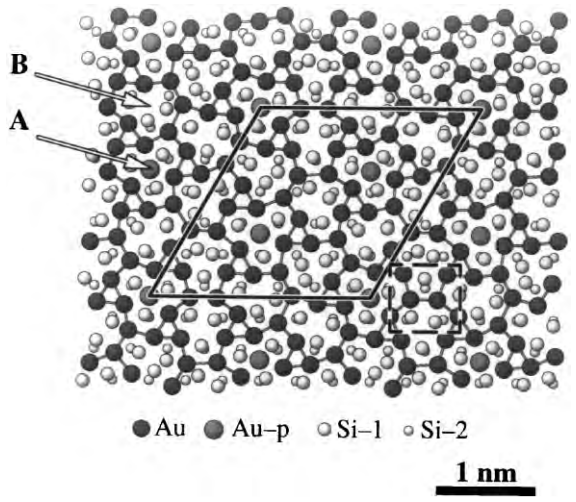

Fig. 5. Diagram of the structure, with the primitive unit cell indicated by solid lines and the notation Au-p for the partially occupied sites. The second double layer silicon atoms are only slightly displaced from bulk sites — see Table 1. The structure can be described in terms of incomplete pentagons and trimer units, or the two gold ring configurations A and B discussed in the text. One of the rectangular units observed in domain boundaries of the $\sqrt{3}\times\sqrt{3}$ structure is shown.

calculated and used to estimate the effect of placing a new atom in a suggested site.

Shown in Fig. 2a is an initial fragment with about 20 gold atoms, found among the top phasing solutions using $p3$ symmetry. Including the peak at the origin which turned out to be only partially occupied, the peaks are very close to gold positions in the final refinement, and three weaker silicon peaks are also observable. Other maps showed different fragments of the total structure. For reference, in $p3$ symmetry incoherent twin domains were assumed yielding $p6mm$ Patterson symmetry. While not obvious in the initial stages of the analysis, all the top solutions in both $p3$ and $p31m$ symmetry showed 20 or more of the gold atoms. Building from this structure we were able to generate the gold framework shown in Fig. 2d, a total of 14 independent sites (42 atoms without the partially occupied sites). Intermediate steps in constructing the model are shown in Fig. 2b and c, with corresponding diffraction patterns in Fig. 3a–d. Fig. 4 shows missing sites suggested by heavy-atom holography applied to the partial model from Fig. 2c; the most intense symmetry equivalent three spots were chosen as the next step (one of them is arrowed in the figure).

As the final step, the atomic positions determined from heavy-atom holography analysis were refined using a conventional χ^2 minimization. In terms of an R-factor defined as:

$$R\equiv\frac{\sum_{j=1}^{N}|I_j^{\mathrm{meas}}-I_j^{\mathrm{calc}}|}{\sum_{j=1}^{N}I_j^{\mathrm{meas}}} \tag{1}$$

where I^{meas} is a measured intensity, I^{calc} is the simulated intensity, and N is the total number of measured intensities, and a reduced χ^n as:

$$\chi^n\equiv\frac{1}{N-M}\sum_{j=1}^{N}\frac{(|I_j^{\mathrm{meas}}-I_j^{\mathrm{calc}}|)^n}{\sigma_j} \tag{2}$$

where M is the number of variables in the refinement and σ_j is the uncertainty in the jth measured intensity, this structure gave $R=0.25$ and $\chi^2=50$. While the χ^2 value is rather high, it is more than two orders of magnitude better than that found in a previous analysis [5]. A strong possibility exists that the experimental results were obtained from a two-phase $\sqrt{3}\times\sqrt{3}$ and 6×6 mixture; eliminating reflections which overlap with the $\sqrt{3}\times\sqrt{3}$ reduced χ^2 to 32 and R to 0.2. (This reduced the number of reflections, in $p3$ plane group, from 248 to 234.) Adding a double silicon layer reduced χ^2 and R again by about a factor of two; similarly, a second double silicon layer reduced χ^2 to about 8.

Based upon previous work [2] with $\sqrt{3}\times\sqrt{3}$, the relaxation extends several layers into the substrate. However, in $p3$ symmetry there are only 234 reflections (about half of these independent), so including large numbers of silicon atoms (12 per layer) is not justifiable in terms of the number of measurements. To compensate for not including independent variables for all subsurface atom positions, a subsurface strain field expanded as the gradient of a two-dimensionally periodic harmonic [36,37] was used to model displacements into the substrate. The strain field is constrained to decay exponentially into the bulk. For the final stages of the minimization, the more robust form χ was utilized. This corresponds to $n=1$ in Eq. (1), and

Table 1
Average atomic positions with 14 gold sites and two Si double layers (24 sites). Only two-dimensional diffraction data were available, so no heights could be refined. Values for the errors (δX, δY) as well as the displacements from bulk sites for the subsurface silicon atoms (ΔX, ΔY) are given. Gold Debye–Waller factor (B) = 1.98 (0.02); occupancy of special (protrusion) sites = 0.504 (0.004)

X	δX	Y	δY		
Gold sites					
0.3435	(0.0012)	0.8670	(0.0005)		
0.3090	(0.0005)	0.3018	(0.0002)		
0.1852	(0.0006)	0.1804	(0.0011)		
0.8647	(0.0004)	0.3488	(0.0003)		
0.2545	(0.0005)	0.0315	(0.0008)		
0.4470	(0.0007)	0.3553	(0.0005)		
0.9560	(0.0003)	0.0926	(0.0007)		
0.6276	(0.0003)	0.2048	(0.0005)		
0.4712	(0.0004)	0.8840	(0.0005)		
0.0089	(0.0006)	0.3582	(0.0001)		
0.2501	(0.0003)	0.7164	(0.0015)		
0.7832	(0.0003)	0.8687	(0.0002)		
0.4523	(0.0008)	0.2356	(0.0007)		
0.5880	(0.0004)	0.8725	(0.0003)		
X	δX	ΔX (Å)	Y	δY	ΔY (Å)
Silicon layer 1					
0.0309	(0.0021)	−0.569	0.9320	(0.0026)	−0.286
0.4116	(0.0009)	0.524	0.6237	(0.0014)	0.291
0.7445	(0.0014)	0.512	0.3147	(0.0032)	0.850
0.3681	(0.0024)	−0.478	0.1072	(0.0006)	−0.090
0.3577	(0.0043)	−0.719	0.2350	(0.0021)	−0.985
0.2369	(0.0036)	0.338	0.1390	(0.0083)	0.643
0.1960	(0.0031)	−0.604	0.3002	(0.0042)	0.517
0.1738	(0.0024)	−1.115	0.3970	(0.0017)	−1.093
0.0908	(0.0008)	0.812	0.3398	(0.0021)	1.428
0.5261	(0.0010)	−0.679	0.4502	(0.0008)	0.133
0.5798	(0.0049)	0.558	0.5665	(0.0049)	−1.027
0.3955	(0.0010)	0.152	0.4152	(0.0015)	−0.674
Silicon layer 2					
0.0582	(0.0002)	0.060	0.1099	(0.0007)	−0.028
0.2220	(0.0004)	−0.005	0.6090	(0.0001)	−0.049
0.7198	(0.0001)	−0.056	0.4453	(0.0012)	0.019
0.2249	(0.0006)	0.061	0.1144	(0.0002)	0.076
0.3882	(0.0007)	−0.015	0.1113	(0.0007)	0.004
0.3870	(0.0010)	−0.044	0.2756	(0.0006)	−0.050
0.0570	(0.0002)	0.033	0.2832	(0.0006)	0.125
0.2211	(0.0002)	−0.027	0.2794	(0.0007)	0.038
0.2189	(0.0001)	−0.077	0.4392	(0.0007)	−0.122
0.3926	(0.0007)	0.086	0.4408	(0.0008)	−0.083
0.5545	(0.0014)	−0.024	0.4469	(0.0015)	0.057
0.5591	(0.0010)	0.081	0.6086	(0.0010)	−0.057

is analogous to a χ^2 analysis with an assumption of exponentially distributed errors between the measurements and the simulations replacing the Gaussian distributed errors assumed in a χ^2 analysis. The χ factor is similar to χ^2 and for a reasonable fit will tend to 1, but it is less sensitive to outliers

Table 2
List of the intensities of the reflections (using crystallographic notation, not fractional indices), the corresponding calculated values, the weighted error and absolute errors for $\chi^2 = 3.8$

H	K	Exp.	Calc.	Wt. error	Abs. error
7	2	0.488×10^2	0.489×10^2	-0.330×10^{-1}	-0.134×10^{-1}
8	1	0.469×10^2	0.449×10^2	0.285×10	0.200×10
9	0	0.311×10^2	0.304×10^2	0.241×10	0.767
7	3	0.229×10^2	0.228×10^2	0.254	0.866×10^{-1}
9	7	0.208×10^2	0.205×10^2	0.556	0.279
5	5	0.175×10^2	0.173×10^2	0.609	0.190
6	3	0.128×10^2	0.131×10^2	-0.132×10	-0.344
4	3	0.117×10^2	0.120×10^2	-0.183×10	-0.296
8	0	0.862×10	0.896×10	-0.132×10	-0.345
9	1	0.937×10	0.964×10	-0.995	-0.263
11	5	0.122×10^2	0.124×10^2	-0.608	-0.179
13	2	0.111×10^2	0.111×10^2	-0.580×10^{-1}	-0.174×10^{-1}
14	1	0.993×10	0.119×10^2	-0.303×10	-0.195×10
10	6	0.873×10	0.883×10	-0.462	-0.993×10^{-1}
10	7	0.810×10	0.768×10	0.190×10	0.421
16	1	0.793×10	0.817×10	-0.595	-0.238
7	5	0.718×10	0.610×10	0.437×10	0.108×10
6	5	0.689×10	0.454×10	0.184×10	0.235×10
15	4	0.596×10	0.642×10	-0.118×10	-0.460
15	0	0.592×10	0.622×10	-0.922	-0.298
3	5	0.584×10	0.598×10	-0.599	-0.143
14	0	0.574×10	0.710×10	-0.451×10	-0.136×10
13	3	0.563×10	0.451×10	0.369×10	0.112×10
9	9	0.552×10	0.528×10	0.101×10	0.241
12	5	0.546×10	0.528×10	0.533	0.178
14	3	0.516×10	0.487×10	0.814	0.296
11	7	0.514×10	0.455×10	0.147×10	0.597
16	3	0.484×10	0.602×10	-0.296×10	-0.119×10
16	0	0.483×10	0.534×10	-0.139×10	-0.517
14	7	0.461×10	0.524×10	-0.183×10	-0.632
11	6	0.460×10	0.417×10	0.161×10	0.438
17	0	0.452×10	0.547×10	-0.191×10	-0.945
13	9	0.405×10	0.309×10	0.346×10	0.963
15	1	0.403×10	0.416×10	-0.407	-0.135
7	4	0.382×10	0.347×10	0.187×10	0.351
6	4	0.367×10	0.324×10	0.143×10	0.426
3	3	0.359×10	0.427×10	-0.337×10	-0.683
14	4	0.355×10	0.334×10	0.627	0.218
10	9	0.346×10	0.362×10	-0.954	-0.161
14	6	0.344×10	0.202×10	0.435×10	0.142×10
7	1	0.336×10	0.447×10	-0.352×10	-0.111×10
10	1	0.336×10	0.328×10	0.519	0.798×10^{-1}
10	5	0.335×10	0.323×10	0.653	0.122
13	8	0.326×10	0.340×10	-0.376	-0.131
9	8	0.308×10	0.248×10	0.253×10	0.597
15	5	0.304×10	0.243×10	0.179×10	0.616
4	1	0.303×10	0.336×10	-0.183×10	-0.333
12	3	0.293×10	0.222×10	0.130×10	0.702
7	7	0.282×10	0.330×10	-0.262×10	-0.481
15	6	0.278×10	0.276×10	0.663×10^{-1}	0.239×10^{-1}
9	2	0.274×10	0.276×10	-0.193	-0.143×10^{-1}

Table 2 (*continued*)

H	*K*	Exp.	Calc.	Wt. error	Abs. error
12	8	0.267×10	0.266×10	0.179	0.120×10^{-1}
10	0	0.244×10	0.235×10	0.540	0.951×10^{-1}
11	4	0.240×10	0.230×10	0.575	0.987×10^{-1}
11	9	0.242×10	0.220×10	0.687	0.223
17	5	0.237×10	0.289×10	-0.139×10	−0.525
16	7	0.224×10	0.220×10	0.149	0.327×10^{-1}
9	4	0.216×10	0.220×10	−0.225	-0.364×10^{-1}
17	7	0.214×10	0.167×10	0.889	0.470
16	2	0.214×10	0.217×10	-0.927×10^{-1}	-0.361×10^{-1}
15	7	0.202×10	0.156×10	0.117×10	0.465
12	10	0.199×10	0.134×10	0.283×10	0.648
15	8	0.189×10	0.988	0.222×10	0.899
10	8	0.184×10	0.201×10	-0.114×10	−0.173
13	5	0.181×10	0.176×10	0.133	0.465×10^{-1}
8	7	0.179×10	0.152×10	0.140×10	0.272
11	11	0.171×10	0.155×10	0.731	0.160
11	1	0.171×10	0.166×10	0.402	0.524×10^{-1}
11	10	0.160×10	0.126×10	0.147×10	0.335
6	2	0.156×10	0.123×10	0.200×10	0.330
6	1	0.150×10	0.168×10	-0.141×10	−0.183
5	2	0.149×10	0.163×10	-0.131×10	−0.142
12	4	0.149×10	0.105×10	0.104×10	0.434
16	6	0.148×10	0.133×10	0.361	0.148
13	7	0.146×10	0.126×10	0.630	0.201
7	6	0.144×10	0.993	0.298×10	0.443
12	9	0.137×10	0.149×10	−0.381	−0.123
18	1	0.130×10	0.160×10	−0.877	−0.297
10	3	0.122×10	0.109×10	0.111×10	0.122
12	1	0.121×10	0.144×10	-0.107×10	−0.228
13	4	0.121×10	0.212×10	-0.283×10	−0.906
8	5	0.118×10	0.112×10	0.365	0.565×10^{-1}
14	9	0.117×10	0.144×10	−0.685	−0.273
9	6	0.110×10	0.130×10	-0.146×10	−0.200
11	3	0.110×10	0.127×10	-0.134×10	−0.164
17	1	0.106×10	0.693	0.750	0.369
17	6	0.105×10	0.783	0.673	0.268
11	2	0.992	0.120×10	-0.161×10	−0.207
15	3	0.976	0.152×10	-0.150×10	−0.546
13	1	0.910	0.112×10	−0.959	−0.205
16	5	0.852	0.118×10	−0.929	−0.331
11	0	0.793	0.723	0.611	0.694×10^{-1}
18	5	0.770	0.143×10	-0.271×10	−0.663
16	8	0.766	0.110×10	−0.810	−0.333
12	2	0.730	0.364	0.153×10	0.366
13	0	0.718	0.883×10^{-1}	0.271×10	0.629
15	9	0.642	0.948	−0.637	−0.306
8	6	0.642	0.356	0.249×10	0.285
8	4	0.633	0.902	-0.225×10	−0.269
13	6	0.631	0.732	−0.291	−0.100
12	7	0.623	0.621	0.654×10^{-2}	0.204×10^{-2}
17	2	0.565	0.122×10	-0.162×10	−0.652
3	1	0.552	0.467	0.174×10	0.854×10^{-1}
5	4	0.513	0.827	-0.168×10	−0.314

Table 2 (*continued*)

H	*K*	Exp.	Calc.	Wt. error	Abs. error
15	2	0.508	0.119×10	-0.183×10	-0.679
13	10	0.484	0.201	0.112×10	0.282
9	3	0.451	0.638	-0.150×10	-0.187
18	2	0.447	0.548	-0.384	-0.101
3	2	0.424	0.429	$-.0110$	-0.471×10^{-2}
18	3	0.400	0.338	0.286	0.616×10^{-1}
19	0	0.372	0.367	0.174×10^{-1}	0.483×10^{-2}
9	5	0.345	0.271	0.646	0.742×10^{-1}
8	3	0.330	0.263	0.112	0.673×10^{-1}
18	4	0.319	0.578	-0.126×10	-0.259
13	11	0.293	0.104×10	-0.297×10	-0.745
11	8	0.245	0.430	-0.586	-0.185
13	11	0.293	0.104×10	-0.297×10	-0.745
11	8	0.245	0.430	-0.586	-0.185
4	2	0.230	0.307	-0.155×10	-0.775×10^{-1}
3	0	0.221	0.254	-0.114×10	-0.334×10^{-1}
12	11	0.215	0.655	-0.138×10	-0.440
1	0	0.203	0.222	-0.301×10	-0.521×10^{-1}
1	1	0.161	0.213	-0.301×10	-0.521×10^{-1}
17	3	0.156	0.250	-0.266	-0.949×10^{-1}
4	0	0.146	0123	0.576	0.224×10^{-1}
2	1	0.980×10^{-1}	0.423×10^{-1}	0.221×10	0.557×10^{-1}
2	0	0.785×10^{-1}	0.500×10^{-1}	0.137×10	0.285×10^{-1}
5	0	0.317×10^{-1}	0.893×10^{-1}	-0.811	-0.576×10^{-1}
14	10	0.219×10^{-1}	0.384	-0.108×10	-0.362
7	0	0.000	0.138	-0.431	-0.138

in the data, points with large errors [38]. For one double layer of silicon we obtained $\chi=2.7$; for two $\chi=2.0$. Including partial occupancy at the three special sites (0, 0), (1/3, 2/3) and (2/3, 1/3) and the subsurface strain field had a large effect, yielding $\chi^2=3.8$ and $\chi=1.7$, with a partial occupancy of approximately 0.5 (total coverage 1.2 ML).

Atom positions for two silicon double layers and the calculated and experimental intensity values are shown in Tables 1 and 2 respectively, and the final model including Au and Si atoms in Fig. 5. For the atom positions we averaged four calculations, two each using χ^2 and χ, with two different registries for the third double layer of silicon atoms, then used these to determine the errors. The gold site errors are about 0.01 Å, the silicon about 0.05 Å. However, since the gold Debye–Waller factor refined to a rather high value (0.16 Å RMS displacement), implying substantial static disorder (consistent with partial occupancy), a multiplicative factor of two to three on the errors might be appropriate. Most of this is almost certainly rotation of the gold trimers, similar to the $\sqrt{3}\times\sqrt{3}$ [2]. We were not able to refine the surface silicon Debye–Waller term which tended to drop to unreasonable values, implying more subsurface relaxations than can reasonably be matched with the available data.

4. Discussion

The most interesting aspects of the structure are that it is astonishingly simple, and at the same time complicated. There is a strong relationship to the parent $\sqrt{3}\times\sqrt{3}$ with three sets of three gold trimers. More interesting is the structure of the additional gold atoms which form incomplete pentagons and trimer units; if all the special sites were occupied, complete pentagons would be formed. Every gold–gold separation is close to

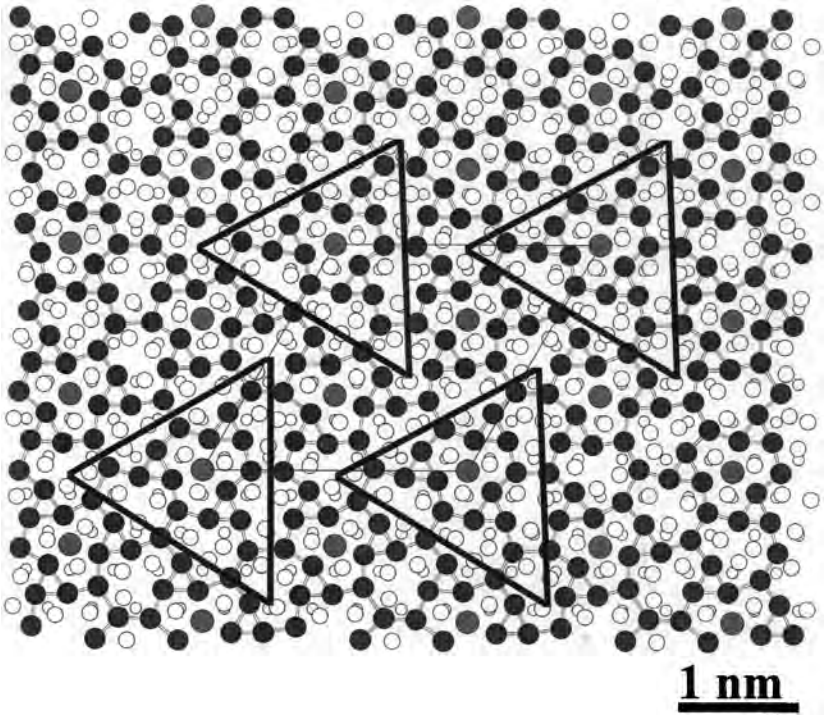

Fig. 6. Triangular domain walls of Si(111)-(6×6)Au, indicated by solid lines.

0.28 nm, the bulk gold interatomic distance. At the center of these incomplete pentagons, probably at the lower apex of a pentagonal prism, are the silicon atoms of the next layer. In a number of cases silicon atoms are separated by about 0.2 nm, implying the presence of second-layer dimerization.

The correspondence at a qualitative level between the structure and the STM images [9,12,39] at lower coverages is good. Similar to the parent $\sqrt{3}\times\sqrt{3}$ structure, the trimers are not properly resolved, and the protrusions are the partially occupied special sites — these match the STM images not only in location within the unit cell but also in terms of their local symmetry. The overall symmetry of the structure is close to $p31m$, again matching well the STM images. The trimers are arranged in rectangular arrays (Fig. 5) which have previously been observed in the domain walls in the $\sqrt{3}\times\sqrt{3}$ structure, where they become more abundant with increasing coverage [9] and the $\sqrt{3}\times\sqrt{3}$ LEED pattern more diffuse. This suggests that the domain walls in the $\sqrt{3}\times\sqrt{3}$ break up with increasing coverage and reorganize as part of the 6×6 structure.

This structure is remarkably similar to what would be expected for a two-dimensional glass with pentagonal units, trimers, and a fixed gold–gold separation. To understand this, note that the structure can be considered as a combination of the two Au ring structures A and B in Fig. 5 surrounding three silicon atoms in the next layer, with two rotational variants of B. The centers of A rings correspond to the partially occupied special sites, and for full occupancy the Au coverage will vary from 1.2 ML to 1.25 ML. Furthermore, filling the center of all B rings will increase the Au coverage to 1.5 ML, thus correlating with the experimental observations of the 6×6 structure's presence for coverages from around 1.0 ML up to 1.5 ML [4,8,9]. Both rings sit at $\sqrt{3}\times\sqrt{3}$ lattice sites, the particular configuration shown giving the 6×6 structure with triangular domain walls consisting of arrays of B rings surrounding A units

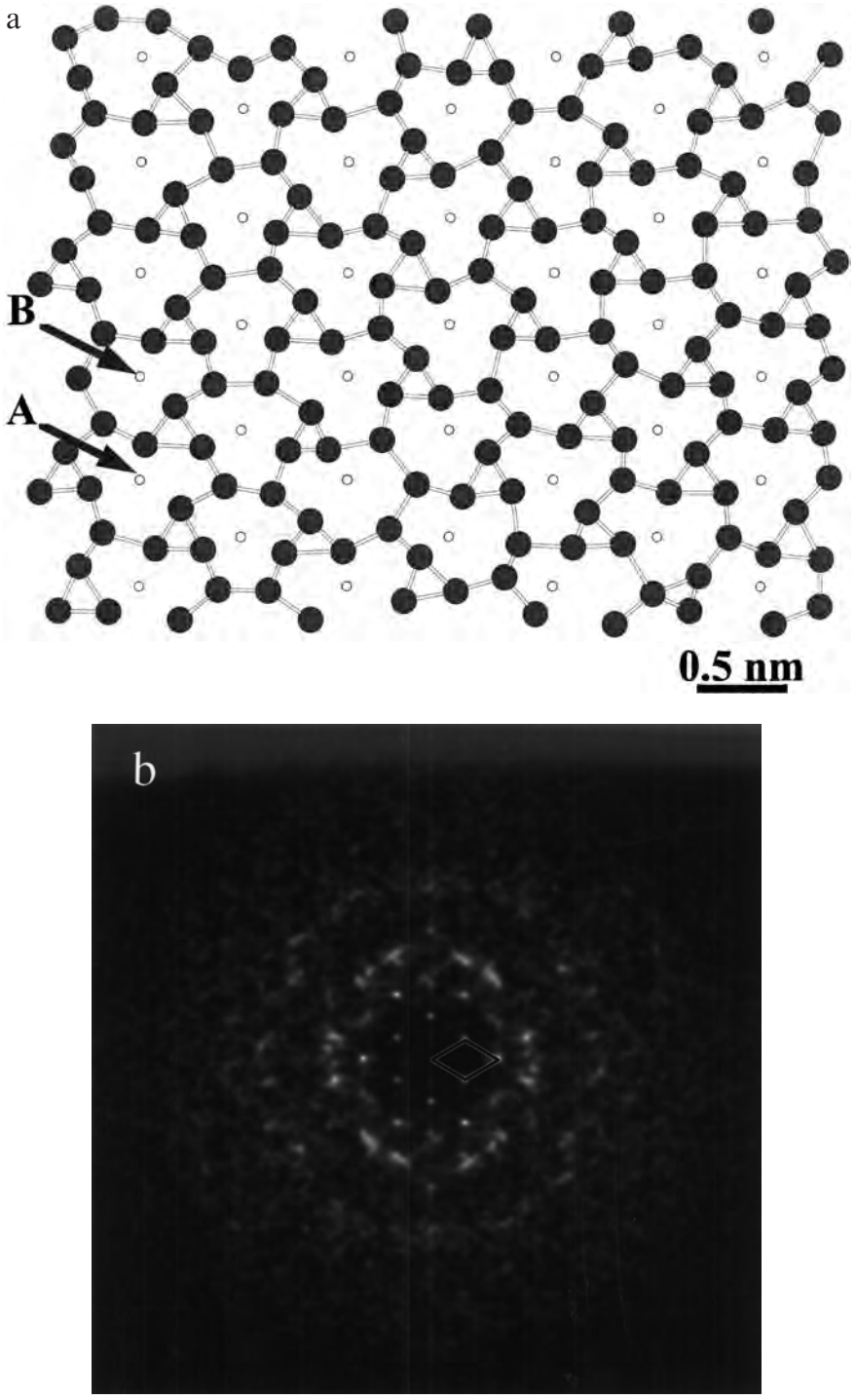

Fig. 7. (a) Glass-like tiling using A and B gold units (Au atoms are large dark circles, and the small empty circles mark the $\sqrt{3}\times\sqrt{3}$ lattice); (b) corresponding diffraction pattern showing sharp diffraction spots at the $\sqrt{3}\times\sqrt{3}$ unit cell reciprocal lattice points and diffuse scattering elsewhere. A $\sqrt{3}\times\sqrt{3}$ unit cell is marked.

(Fig. 6). Pure A units (with vacancies) will give the known $\sqrt{3}\times\sqrt{3}$ structure. Other tilings will yield a combination of trimers and incomplete pentagon units breaking the long-range order to produce a glass-like structure. However, this would not be a true glass because relatively sharp diffraction spots will be obtained at the $\sqrt{3}\times\sqrt{3}$ unit cell reciprocal lattice points, with diffuse scattering elsewhere, in agreement with experimental data [4–9]. A glass-like tiling using A and B gold units sitting at $\sqrt{3}\times\sqrt{3}$ lattice sites and its corresponding diffraction pattern are shown in Fig. 7. We hypothesize that the whole coverage range 0.8–1.5 ML is really a surface solution pseudo-glass. As such it is a two-dimensional analogue of the bulk glassy state, which may well have similar structural units.

Many questions remain open about this structure. It would obviously be good to obtain more precise information about the silicon sites, which would require collection of a larger data set using either X-ray or transmission electron diffraction. {Electron diffraction will be more sensitive to the silicon sites, e.g. the case of the Si(111)-($\sqrt{3}\times\sqrt{3}$)R30°Ag reconstruction, where all Ag and Si sites are clearly visible in the phasing maps [35].} We also suspect that there may be other ordered structures, and there is some evidence already for this from electron diffraction, LEED [Si(111)-($2\sqrt{3}\times 2\sqrt{3}$)Au] [7], RHEED [Si(111)-($2\sqrt{21}\times 2\sqrt{21}$)R10.9°Au] [10], and STM data [9]. Aside from the structural aspects, an intriguing question is the character of the electronic states in this two-dimensional structure. In addition to standard surface spectroscopic techniques, matching the already available STM data at different biases with theoretical calculations would be very interesting.

Acknowledgements

This work was supported by the National Science Foundation (LDM and DG) under Grant Number #DMR-9214505.

References

[1] L.D. Marks, R. Plass, Phys. Rev. Lett. 75 (1995) 2172 and references cited therein.
[2] R. Plass, L.D. Marks, Surf. Sci. 342 (1995) 233 and references cited therein.
[3] R. Plass, L.D. Marks, Surf. Sci. 380 (1997) 497.
[4] K. Higashiyama, S. Kono, T. Sagawa, Jpn. J. Appl. Phys. 25 (1986) L117.
[5] D. Dornisch, W. Moritz, H. Schulz, R. Feidenhans'l, M. Nielsen, F. Grey, R.L. Johnson, Phys. Rev. B 44 (1991) 11221.
[6] S. Takahashi, Y. Tanashiro, K. Takayanagi, Surf. Sci. 242 (1991) 73.
[7] J. Yuhara, M. Inoue, K. Morita, J. Vac. Sci. Technol. A 10 (1992) 334.
[8] J. Yuhara, M. Inoue, K. Morita, J. Vac. Sci. Technol. A 10 (1992) 3486.
[9] T. Takami, D. Fukushi, T. Nakayama, M. Uda, M. Aono, Jpn. J. Appl. Phys. 33 (1994) 3688.
[10] E.A. Khramtsova, A. Ichimiya, Jpn. J. Appl. Phys. 36 (1997) L926.
[11] J.H. Huang, R.S. Williams, Phys. Rev. B 38 (1988) 4022.
[12] J. Nogami, A.A. Baski, C.F. Quate, Phys. Rev. Lett. 65 (1990) 1611.
[13] G. Le Lay, G. Quentel, J.P. Faurie, A. Mason, Thin Solid Films 35 (1976) 273.
[14] W. Święch, E. Bauer, M. Mundschau, Surf. Sci. 253 (1991) 283.
[15] W.K. Klement, R.H. Willens, P. Duwez, Nature 187 (1960) 869.
[16] H. Okamoto, T.B. Massalski, Bull. Alloy Phase Diagr. 4 (1983) 190.
[17] W. Robinson, R. Sharma, L. Eyring, Acta Metall. Mater. 39 (1991) 179.
[18] F.H. Baumann, W. Schroter, Phys. Rev. B 43 (1991) 6510.
[19] A. Hiraki, M. Iwami, Jpn. J. Appl. Phys. Suppl. 2 (1974) 749.
[20] A.K. Green, E. Bauer, J. Appl. Phys. 47 (1976) 1284.
[21] A. Ichimiya, H. Nomura, Y. Ito, H. Iwashige, J. Cryst. Growth 150 (1995) 1169.
[22] G.D. Wilk, R.E. Martinez, J.F. Chervinsky, F. Spaepen, J.A. Golovchenko, Appl. Phys. Lett. 65 (1994) 866.
[23] J.J. Lander, Surf. Sci. 1 (1964) 125.
[24] F. Salvan, H. Fuchs, A. Baratoff, G. Binning, Surf. Sci. 162 (1985) 634.
[25] L.D. Marks, D. Grozea, R. Feidenhans'l, M. Nielsen, R.L. Johnson, Surf. Rev. Lett. 5 (1998) 459.
[26] M.M. Woolfson, Acta Crystallogr. A3 (1987) 593.
[27] D.L. Dorset, Structural Electron Crystallography, Plenum Press, New York, 1995.
[28] L.D. Marks, R. Plass, D. Dorset, Surf. Rev. Lett. 4 (1997) 1.
[29] C. Collazo-Davila, L.D. Marks, K. Nishii, Y. Tanishiro, Surf. Rev. Lett. 4 (1997) 65.

[30] C.J. Gilmore, L.D. Marks, D. Grozea, C. Collazo-Davila, E. Landree, R.D. Twesten, Surf. Sci. 381 (1997) 77.
[31] C. Collazo-Davila, D. Grozea, L.D. Marks, Phys. Rev. Lett. 80 (1998) 1678.
[32] E. Landree, C. Collazo-Davila, L.D. Marks, Acta Crystallogr. B53 (1997) 916.
[33] L.D. Marks, E. Landree, Acta Crystallogr. A54 (1998) 296.
[34] L.D. Marks, E. Bengu, C. Collazo-Davila, D. Grozea, E. Landree, C. Leslie, W. Sinkler, Surf. Rev. Lett. (1998) in press.
[35] D. Grozea, E. Landree, C. Collazo-Davila, E. Bengu, R. Plass, L.D. Marks, Micron (1998) in press.
[36] G. Jayaram, P. Xu, L.D. Marks, Phys. Rev. Lett. 71 (1993) 3489.
[37] A.E.H. Love, A Treatise on the Mathematical Theory of Elasticity, Dover, New York, 1944, p. 172.
[38] W.H. Press, B.F. Flannery, S.A. Teukolsky, W.T. Vetterling, Numerical Recipes, Cambridge University Press, Cambridge, 1986, p. 539.
[39] J. Falta, A. Hille, D. Novikov, G. Materlik, L. Seehofer, G. Falkenberg, R.L. Johnson, Surf. Sci. 330 (1995) L673.